PHYSICAL REVIEW D **87,** 095012 (2013)

# Higgs boson mass, proton decay, naturalness, and constraints of the LHC and Planck data

Mengxi Liu* and Pran Nath†

*Department of Physics, Northeastern University, Boston, Massachusetts 02115, USA*

(Received 29 March 2013; published 20 May 2013)

A Higgs boson mass ∼126 GeV as determined by the LHC data requires a large loop correction, which in turn implies a large sfermion mass. Implication of this result for the stability of the proton in supersymmetric grand unified theories is examined including other experimental constraints along with the most recent result on cold dark matter from Planck. It is shown that over the allowed parameter space of supergravity unified models, proton lifetime is highly sensitive to the Higgs boson mass and a few GeV shift in its mass can change the proton decay lifetime for the mode $p \to \bar{\nu} K^+$ by as much as two orders of magnitude or more. An analysis is also given on the nature of radiative breaking of the electroweak symmetry in view of the high Higgs boson, and it is shown that most of the parameter space of universal and nonuniversal supergravity unified models lies on the hyperbolic branch of radiative breaking of the electroweak symmetry, while the ellipsoidal branch and the focal point regions are highly depleted and contain only a very small region of the allowed parameter space. Also discussed are the naturalness criteria when the proton stability constraints along with the electroweak symmetry breaking are considered together. It is shown that under the assumed naturalness criteria, the overall fine-tuning is improved for larger values of the scalar mass with the inclusion of the proton stability constraint. Thus, the naturalness criteria including proton stability along with electroweak symmetry breaking constraints tend to favor the weak scale of supersymmetry in the several TeV region. Implications for the discovery of supersymmetry in view of the high Higgs mass are briefly discussed.

DOI: 10.1103/PhysRevD.87.095012 PACS numbers: 14.80.Da, 12.60.Jv

## I. INTRODUCTION

Over the past year, the ATLAS and the CMS collaborations have identified a signal for a boson around ∼126 GeV. Thus, the ATLAS Collaboration finds a signal at $126.0 \pm 0.4(\text{stat}) \pm 0.4(\text{sys})$ GeV, which is at the $5.0\sigma$ level [1] while the CMS Collaboration finds a signal at $125.3 \pm 0.4(\text{stat}) \pm 0.5(\text{sys})$ GeV at the $5.0\sigma$ level [2]. While the properties of the new boson still need to be fully established, it is widely believed that the discovered boson is indeed the Higgs boson [3–5] that enters in the breaking of the electroweak symmetry of the Standard Model [6,7]. Remarkably, the Higgs boson mass lies close to the upper limit predicted in supergravity grand unified models [8–11], which predict an upper limit of around 130 GeV [12–16] (for a recent review of Higgs and supersymmetry (SUSY), see Ref. [17]). The high mass ∼126 GeV requires a large loop correction, which in turn implies that some of the sparticles entering the loop corrections (for a review, see Ref. [18]) to the Higgs mass must be in the several TeV range. In this case the heavy particles could be out of reach of the LHC. One possibility is that a part of the Higgs boson arises from sources outside of the minimal supersymmetric Standard Model such as from corrections arising from vectorlike multiplets [19–22]. However, in this work we do not make that assumption.

In the early analyses using radiative breaking of the electroweak symmetry (for a review, see Ref. [23]), only the ellipsoidal branch was known, in that a fixed value of the $\mu$ (the Higgs mixing parameter) implied upper limits on sparticle masses. However, the situation changed drastically with the discovery of the hyperbolic branch [24,25] (for related work, see Refs. [26,27]) when it was discovered that another branch of radiative breaking of the electroweak symmetry existed in which the sparticle masses could lie in the several TeV region while $\mu$ could still be at the sub-TeV scale. Specifically on this branch, TeV size scalars can exist consistent with small $\mu$. In this work we investigate the allowed parameter space of supergravity models under the constraint that the models accommodate the high Higgs mass. We show that for supergravity models, most of the allowed parameter space under the high Higgs mass restriction lies on the hyperbolic branch (HB) while the ellipsoidal branch (EB) and focal point (FP) region accommodate only a small fraction of the allowed parameter space. We discuss the above for supergravity models with universal boundary conditions (minimal supergravity grand unification/constrained minimal supersymmetric standard model (mSUGRA/CMSSM)) as well as supergravity models with nonuniversal gaugino masses (supergravity grand unified models with nonuniversalities (NuSUGRA)). Sensitivity of the proton lifetime to the Higgs boson mass is investigated, and it is shown that the proton lifetime is correlated very sensitively to the Higgs boson mass. Further, we discuss issues of naturalness in view of the large Higgs boson mass and the stability of the proton. It is shown that a composite

*m.liu@neu.edu
†nath@neu.edu

 

fine-tuning including proton stability along with the radiative electroweak symmetry breaking constraint prefers a SUSY scale in the several TeV region.

The outline of the rest of the paper is as follows. In Sec. II we discuss the radiative breaking of the electroweak symmetry under the constraint of the high Higgs boson mass. Here, we show that most of the parameter space of supergravity unified models with universal boundary conditions lies on the hyperbolic branch while the ellipsoidal branch and the focal point region are essentially empty. In Sec. III we discuss the implications of the high Higgs boson mass on the proton lifetime and show that the proton lifetime is very sensitive to small shifts in the Higgs boson mass. Thus, a shift of a few GeV of the light Higgs boson mass can change the proton lifetime by as much as 2 orders of magnitude or more. In Sec. IV we extend the discussion to supergravity unified models with nonuniversalities and show that the broad conclusions drawn in the previous sections still hold. In Sec. V we discuss the issue of naturalness and fine-tuning when the proton stability constraints are combined with the constraints from electroweak symmetry breaking. Here, it is shown that the fine-tuning criteria including both the proton stability and the electroweak symmetry breaking constraints favor a high sfermion scale. Conclusions are given in Sec. VI.

## II. HIGGS MASS AND BRANCHES OF RADIATIVE BREAKING OF THE ELECTROWEAK SYMMETRY

It is of interest to investigate the allowed parameter space of the supergravity unified models under the constraint of the high Higgs boson mass. We consider first supergravity unified models with universal boundary conditions consisting of the universal scalar mass $m_0$; universal gaugino mass $m_{1/2}$; universal trilinear coupling $A_0$, $\tan\beta = \langle H_2\rangle/\langle H_1\rangle$, where $H_2$ gives mass to the up quarks and $H_1$ gives mass to the down quarks and leptons; and the Higgs mixing parameter $\mu$, which enters the superpotential via the term $\mu H_1 H_2$. Of specific interest is to determine the branch of radiative breaking of the electroweak symmetry preferred by the high mass. Thus, the radiative electroweak symmetry breaking can be exhibited in the following form [24,28]:

$$\mu^2 + \frac{1}{2}M_Z^2 = m_0^2 C_1 + A_0'^2 C_2 + m_{1/2}^2 C_3' + \Delta\mu^2_{\rm loop}, \qquad (1)$$

where $A_o' \equiv A_0 + \frac{C_4}{2C_2} m_{1/2}$ and

$$C_1 = \frac{1}{\tan^2\beta - 1}\left(1 - \frac{3D_0 - 1}{2}\tan^2\beta\right),$$
$$C_2 = \frac{\tan^2\beta}{\tan^2\beta - 1}k, \qquad C_3' \equiv C_3 - \frac{C_4^2}{4C_2}, \qquad (2)$$

$$C_3 = \frac{1}{\tan^2\beta - 1}(g - e\tan^2\beta), \quad C_4 = -\frac{\tan^2\beta}{\tan^2\beta - 1}f. \qquad (3)$$

Here, $e.f$, $g$, and $k$ are as defined in Ref. [29], and $D_0(t)$ is defined by

$$D_0(t) = (1 + 6Y_0 F(t))^{-1}. \qquad (4)$$

In the above $Y_0 = h_t(0)^2/(4\pi^2)$, where $h_t(0)$ is the top Yukawa coupling at the grand unified theory scale (GUT), $M_G \simeq 2\times 10^{16}$ GeV. $F(t)$ is defined by $F(t) = \int_0^t E(t')dt'$, where $E(t) = (1+\beta_3 t)^{16/3b_3}(1+\beta_2 t)^{3/b_2}(1+\beta_1 t)^{13/9b_1}$. Here, $\beta_i = \alpha_i(0)b_i/(4\pi)$ and $b_i = (-3, 1, 11)$ for $SU(3)$, $SU(2)$ and $U(1)$ and $t = \ln(M_G^2/Q^2)$, where $Q$ is the renormalization group point. We are using the normalizations for which $\alpha_3(0) = \alpha_2(0) = \frac{5}{3}\alpha_1(0) = \alpha_G(0)$, and $\alpha_G(0)$ is the common value of the normalized $\alpha' s$ at the GUT scale. Finally, $\Delta\mu^2_{\rm loop}$ is the loop correction [30]. To understand the origin of the branches of radiative breaking, it is useful to choose a renormalization group scale $Q$ where the loop correction $\Delta\mu^2_{\rm loop}$ is minimized. In this circumstance if all the coefficients $C_1$, $C_2$, $C_3'$ are positive, the right-hand side of Eq. (1) is a positive sum of squares, which leads to an upper limit on each of the soft parameters determined by the size of $\mu^2 + \frac{1}{2}M_Z^2$ on the left-hand side. This is the so-called EB, where $\mu$ sets an upper limit on the soft parameters and thus on the size of the sparticle masses. This is typically the case if the loop correction $\Delta\mu^2_{\rm loop}$ is small. However, the situation changes drastically if the loop correction $\Delta\mu^2_{\rm loop}$ is large. This is so because $C_i$ are functions of the renormalization group (RG) scale $Q$, and for the case in which the loop correction $\Delta\mu^2_{\rm loop}$ is large, the RG dependence of $C_i$ can become significant. Indeed, as we change the renormalization group scale $Q$, there is a rapid change in $\Delta\mu^2_{\rm loop}$ and a rapid compensating change also in the remaining terms on the right-hand side of Eq. (1) so that $\mu^2$ does not exhibit any rapid dependence on $Q$. Now it turns out that there are regions of the parameter space in which one or more of the $C_i$ may turn negative as $Q$ varies. For the supergravity unified models with universal boundary conditions, this is the case for $C_1$, i.e., in certain regions of the parameter space, $C_1$ can turn negative while the remainder on the right-hand side of Eq. (1) remains positive. In this case it is useful to write Eq. (1) in the following form:

$$\mu^2 = \begin{pmatrix} +1 & (\rm EB) \\ 0 & (\rm FP) \\ -1 & (\rm HB) \end{pmatrix} m_0^2|C_1| + \Delta^2, \qquad (5)$$

where $\Delta^2$ stands for the rest of the terms in Eq. (1). In Eq. (5) $+1$ corresponds to the EB, $-1$ corresponds to the HB, and $C_1 = 0$ is the boundary point between the two, which we call the FP. Its approximate form when $\tan\beta \gg 1$ is the focus point [31]. $C_1 = 0$ is achieved when $D_0 = 1/3$ (see Appendix A). We wish now to identify the allowed regions of the mSUGRA parameter space in terms of the

branch on which they reside, i.e., EB, HB, or FP. To quantify the region FP, we define a small corridor around $C_1 = 0$. This is feasible since the FP is very sensitive to the top quark mass, and we utilize the error in the top quark mass to define the corridor around $C_1 = 0$. Currently, the top quark mass is determined to be $m_t = (173.5 \pm 1.0)$ GeV, and thus we define the FP corridor so that [32]

$$|C_1| < \delta(Q, m_t), \qquad \delta(Q, m_t) \ll 1, \tag{6}$$

where

$$\delta(Q, m_t) \simeq 3(1 - D_0)\frac{\delta m_t}{m_t}, \tag{7}$$

and where $D_0$ is defined in Eq. (4). Thus, the FP corresponds to the corridor $-|\delta| < C_1 < |\delta|$, the EB corresponds to $C_1 > |\delta|$, and HB corresponds to $C_1 < -|\delta|$. The EB consists of closed elliptical curves and closed surfaces in the soft parameter space for fixed $\mu$, while the HB region $C_1 < -|\delta|$ consists of open curves and open surfaces. We now define a focal curve (FC) on HB as the one on which two soft parameters can get large while $\mu$ remains fixed. It was shown in Ref. [32] that in mSUGRA there exist two varieties of focal curves, FC1 and FC2, as shown in Table I. On FC1 $m_{1/2}$ and $\mu$ remain fixed while $m_0$ and $m_{1/2}$ get large, and thus FC1 is an open curve lying in the $m_0 - A_0$ plane. On FC2 $A_0$ and $\mu$ remain fixed while $m_0$ and $A_0$ get large, and thus FC2 is an open curve lying in the $m_0 - m_{1/2}$ plane. A convolution of focal curves leads to focal surfaces.[1] It is interesting to classify the allowed parameter space of mSUGRA in terms of the branch of radiative breaking of the electroweak symmetry on which they lie, i.e., EB, HB, or FP. This is done under the constraints of the most recent LHC searches [33–37] and other experimental constraints including the most recent results from the Planck experiment [38].

We investigate the issue of classification of the branches of mSUGRA by mapping the soft parameters space in the following ranges: $m_0 \in (200\ \text{GeV}, 30\ \text{TeV})$, $m_{1/2} \in (100\,\text{GeV}, 5\,\text{TeV})$, $A_0 \in (-6m_0, 6m_0)$, and $\tan\beta \in (1, 60)$. Experimental constraints are then applied for all model points including the limits on sparticle masses from the large electron-positron collider [39]: $m_{\tilde{\tau}_1} > 81.9$ GeV, $m_{\tilde{\chi}_1^\pm} > 103.5\,\text{GeV}$, $m_{\tilde{t}_1} > 95.7\,\text{GeV}$, $m_{\tilde{b}_1} > 89\,\text{GeV}$, $m_{\tilde{e}_R} > 107\,\text{GeV}$, and $m_{\tilde{\mu}_R} > 94$ GeV. The most recent Planck measurement [38] of the relic density of cold dark matter gives $\Omega_\chi h^2 = 0.1199 \pm 0.0027$. Here, we apply the $4\sigma$ upper bound, i.e., $\Omega_\chi h^2 < 0.13$. Other constraints applied include the $g_\mu - 2$ constraint $(-11.4 \times 10^{-10}) \leq \delta(g_\mu - 2) \leq (9.4 \times 10^{-9})$ and the flavor-changing neutral current (FCNC) constraint from $B$-physics measurements [40–42], i.e., $(2.77\times10^{-4}) \leq \text{Br}(b\to s\gamma) \leq (4.37\times10^{-4})$ and $\text{Br}(B_s \to \mu^+\mu^-) \leq 1.1 \times 10^{-8}$. As done in Refs. [32,43], we will refer to these constraints as the *general constraints*. These constraints are imposed using MICROMEGAS [44] for the relic density as well as for the indirect constraints and SOFTSUSY [45] for the sparticle mass spectrum. We will also consider NuSUGRA models. (For recent works on NuSUGRA, see Refs. [46–48], and for a review, see Ref. [49]. String-based models also allow for nonuniversalities of gaugino masses; see, e.g., Ref. [50].) The supergravity grand unification formalism of Ref. [8] still applies. For the NuSUGRA case to be discussed in Sec. IV, all of the experimental constraints discussed above still apply except that the ranges of the soft parameters are chosen as follows: $m_0 \in (200\,\text{GeV}, 30\,\text{TeV})$, $m_i \in (100\,\text{GeV}, 5\,\text{TeV})$, $A_0 \in (-6m_0, 6m_0)$, and $\tan\beta \in (1, 60)$ where $i = 1, 2, 3$ for NuSUGRA.

TABLE I. Classification of focal curves in mSUGRA. The focal curve HB/FC1 corresponds to the case in which $m_{1/2}$ is kept fixed while $m_0$ and $A_0$ get large keeping $\mu$ fixed (the asymptotic form of these curves gives $m_0/A_0 = \pm 1$ [27]). The focal curve HB/FC2 corresponds to the case in which $A_0$ and $\mu$ are kept fixed while $m_0$ and $m_{1/2}$ get large.

| Focal curve | Large soft parameters | Small soft parameters |
|---|---|---|
| HB/FC1 | $m_0 - A_0$ | $m_{1/2}$ |
| HB/FC2 | $m_0 - m_{1/2}$ | $A_0$ |

In Fig. 1 we exhibit the allowed parameter space of the supergravity unified models with universal boundary conditions in the $m_0 - m_{1/2}$ plane consistent with all the constraints discussed above. The region excluded by the most recent ATLAS and CMS searches is exhibited. In this figure we also show the regions of the parameter space that lie on the HB, EB, and FP branches of radiative breaking of the electroweak symmetry. The figure shows that essentially all the parameter space of the universal supergravity unified model lies in the HB region (indicated by green points), and the EB region (indicated by red points) and the FP region (indicated by blue points) are essentially both empty except for a few scattered points (see also Ref. [32]). The analysis of Fig. 1 shows that the Higgs mass as well as the FCNC constraints are even stronger than the LHC data on sparticle mass limits. We also note that it is tempting to think that the LHC exclusion plots may be extrapolated beyond $m_0 = 3$ TeV. This region is controlled by the Higgs pole constraint on the relic density [51], which puts limits on the allowed range of the neutralino mass and hence on the gluino mass. The relic density here is insensitive to $m_0$. However, an analysis of the LHC limits beyond 3 TeV depends on knowledge of the backgrounds and on the specifics of the detectors, and a proper analysis

[1]The classification of the parameter space of SUGRA models into focal curves and focal surfaces is a geometric one independent of issues of fine-tuning. The focal curves and focal surfaces automatically arise on HB for the mSUGRA case when $C_1 < 0$. For NuSUGRA the HB gets redefined such that $\mu$ remains constant while two or more soft parameters get large due to one or more of the $C_i$ turning negative as discussed in Sec. IV.

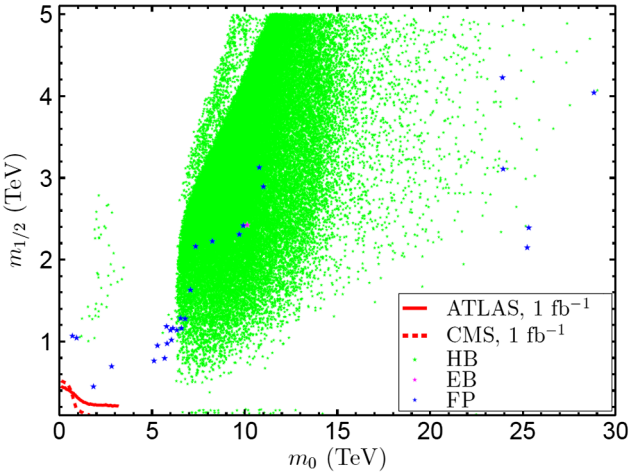


FIG. 1 (color online). The parameter points in the $m_0 - m_{1/2}$ plane in supergravity unified models with universal boundary conditions passing the general constraints. The plot exhibits the parameter points that lie on the HB (green), EB (red), and FP (blue). The analysis shows that most of the allowed parameter space lies on the HB while the allowed regions of the EB and FP are essentially empty except for a few scattered points. For the analysis here and elsewhere in the paper, we have used a top mass of 172.9 GeV. The region excluded by the ATLAS and CMS collaborations is also exhibited.

of this can only be done by the ATLAS and the CMS collaborations.

## III. PROTON STABILITY

In supersymmetric GUTs proton decay from dimension-five operators depends very sensitively on the sparticle spectrum since the sparticle spectrum enters in the dressing loop diagrams which involve the exchange of squarks and sleptons, gluinos, charginos, and neutralinos [52–56] (for recent reviews, see Refs. [57–59]). Thus, low values of sfermion masses can lead to too rapid a proton decay for the mode $p \to \bar{\nu} K^+$ in conflict with the current experimental limit [59], i.e.,

$$\tau^{\rm exp}(p \to \bar{\nu} K^+) > 4 \times 10^{33} \text{ yr}. \tag{8}$$

Since a heavy Higgs boson mass in the vicinity of $\sim$126 GeV implies relatively large values of sfermion masses, it is pertinent to investigate proton stability within the constraint of the experimentally observed large Higgs boson mass. We will limit ourselves to generic $SU(5)$ type models. Further, while chargino $\tilde{\chi}^{\pm}$, gluino $\tilde{g}$, and neutralino $\tilde{\chi}^0$ exchange diagrams all contribute to the decay width, the dominant contribution comes from the chargino exchange diagram, and we will limit ourselves to considerations for decay with this exchange. Thus, here, the decay width is given by Ref. [60],

$$\Gamma(p \to \bar{\nu}_i K^+) = \left(\frac{\beta_p}{M_{H_3}}\right)^2 |A|^2 |B_i|^2 C, \tag{9}$$

where $M_{H_3}$ is the Higgsino triplet mass and $\beta_p$ is the matrix element between the proton and the vacuum state of the three quark operator so that $\beta_p U_L^{\gamma} = \epsilon_{abc}\epsilon_{\alpha\beta}\langle 0|d_{aL}^{\alpha} u_{bL}^{\beta} u_{cL}^{\gamma}|p\rangle$, where $U_L^{\gamma}$ is the proton spinor. The most reliable evaluation of $\beta_p$ comes from lattice gauge calculations and is given Ref. [61] as $\beta_p = 0.0118$ GeV$^3$. Other factors that appear in Eq. (9) have the following meaning: $A$ contains the quark mass and Cabibbo-Kobayashi-Maskawa (CKM) factors, $B_i$ are the functions that describe the dressing loop diagrams, and $C$ contains chiral Lagrangian factors which convert the Lagrangian involving quark fields to the effective Lagrangian involving mesons and baryons. Individually, these functions are given by

$$A = \frac{\alpha_2^2}{2M_W^2} m_s m_c V_{21}^{\dagger} V_{21} A_L A_S, \tag{10}$$

where $m_s(m_c)$ are the strange (charm) quark mass, $V_{ij}$ are the CKM factors, $A_L$ and $A_S$ are the long-distance and the short-distance renormalization group suppression factors as one evolves the operators from the GUT scale down to the electroweak scale and then from the electroweak scale down to 1 GeV [53,62–65], and $B_i$ are given by

$$B_i = \frac{1}{\sin 2\beta} \frac{m_i^d V_{i1}^{\dagger}}{m_s V_{21}^{\dagger}} \left[ P_2 B_{2i} + \frac{m_t V_{31} V_{32}}{m_c V_{21} V_{22}} P_3 B_{3i} \right], \tag{11}$$

where $m_i^d$ is the down quark mass for flavor $i$ and $m_t$ is the top quark mass. Here, the first term in the bracket is the contribution from the second generation, and the second term is the contribution from the third generation, and $P_2$, $P_3$ with values $(\pm 1)$ are the relative parities of the second- and the third-generation contributions. The functions $B_{ji}$ are the loop integrals defined by $B_{ji} = F(\tilde{u}_i, \tilde{d}_j, \tilde{\chi}^{\pm}) + (\tilde{d}_j \to \tilde{e}_j)$, where

$$\begin{aligned} F(\tilde{u}_i, \tilde{d}_j, \tilde{\chi}^{\pm}) &= [E \cos\gamma_- \sin\gamma_+ \tilde{f}(\tilde{u}_i, \tilde{d}_j, \tilde{\chi}_1^{\pm}) \\ &\quad + \cos\gamma_+ \sin\gamma_- \tilde{f}(\tilde{u}_i, \tilde{d}_j, \tilde{\chi}_2^{\pm})] \\ &\quad - \frac{1}{2} \frac{\delta_{i3} m_i^u \sin 2\delta_{ui}}{\sqrt{2} M_W \sin\beta} [E \sin\gamma_- \sin\gamma_+ \tilde{f}(\tilde{u}_{i1}, \tilde{d}_j, \tilde{\chi}_1^{\pm}) \\ &\quad - \cos\gamma_- \cos\gamma_+ \tilde{f}(\tilde{u}_{i1}, \tilde{d}_j, \tilde{\chi}_2^{\pm}) - (\tilde{u}_{i1} \to \tilde{u}_{i2})], \end{aligned} \tag{12}$$

and where $\tilde{f}$ appearing in Eq. (12) is given by

$$\tilde{f}(\tilde{u}_i, \tilde{d}_j, \tilde{\chi}_k^{\pm}) = \sin^2\delta_{ui} f(\tilde{u}_{i1}, \tilde{d}_j, \tilde{\chi}_k^{\pm}) + \cos^2\delta_{ui} f(\tilde{u}_{i2}, \tilde{d}_j, \tilde{\chi}_k^{\pm}). \tag{13}$$

Here, the tilde quantities in the arguments are the sparticle masses, i.e., $\tilde{u}_i$ are the up squark masses for flavor $i$, and $\tilde{d}_j$ are the down squark masses for flavor $j$, and the function $f$ is defined by

$$f(a,b,c) = \frac{m_c}{m_b^2 - m_c^2}\left[\frac{m_b^2}{m_a^2 - m_b^2}\ln\left(\frac{m_a^2}{m_b^2}\right) - (m_a \to m_c)\right]. \quad (14)$$

Further in Eq. (12), $\gamma_\pm = \beta_+ \pm \beta_-$, where $\sin 2\beta_\pm = (\mu \pm m_2)/[4\nu_\pm^2 + (\mu \pm m_2)^2]^{1/2}$, $\sqrt{2}\nu_\pm = M_W(\sin\beta \pm \cos\beta)$, and $\sin 2\delta_{u3} = -2(A_t + \mu\cot\beta)m_t/(m_{\tilde{t}_1}^2 - m_{\tilde{t}_2}^2)$, $E=1$ when $\sin 2\beta > \mu m_2/M_W^2$, and $E=-1$ when $\sin 2\beta < \mu m_2/M_W^2$. Finally, $C$ is given by

$$C = \frac{m_N}{32\pi f_\pi^2}\left[\left(1 + \frac{m_N(D+F)}{m_B}\right)\left(1 - \frac{m_K^2}{m_N^2}\right)\right]^2, \quad (15)$$

where $\tilde{t}_i$ are the stop masses and $f_\pi$, $D$, $F$, etc., are the chiral Lagrangian factors and we use the numerical values $f_\pi = 0.131$ GeV, $D = 0.8$, $F = 0.47$, $m_N = 0.94$ GeV, $m_K = 0.495$ GeV, and $m_B = 1.15$ GeV and we choose $P_2 = 1$ and $P_3 = -1$. The partial decay lifetime of the proton into $p \to \bar{\nu}K^+$ mode is given by $\tau(p \to \bar{\nu}K^+) = \hbar/\Gamma(p \to \bar{\nu}K^+)$.

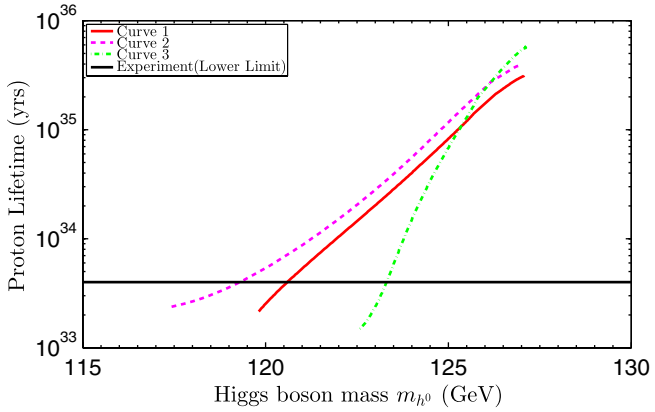


FIG. 2 (color online). An exhibition of the sensitive dependence of the proton lifetime for the decay mode $p \to \bar{\nu}K^+$ as a function of the Higgs boson mass for the supergravity unified model with universal boundary conditions. Parameters for curves 1–3 are as follows. Curve 1: $m_{1/2} = 4207$ GeV, $A_0 = 20823$ GeV, $\tan\beta = 7.3$ while $m_0$ varies, and $M_{H_3}^{\rm eff}/M_G = 50$ here and for other curves. Curve 2: $m_{1/2} = 2035$ GeV, $A_0 = 16336$ GeV, $\tan\beta = 8$ while $m_0$ and $A_0$ vary. Curve 3: $m_{1/2} = 3048$ GeV, $A_0/m_0 = -0.5$, $\tan\beta = 6.5$ while $m_0$ and $A_0$ vary.

Typically, supersymmetric models give too rapid a proton decay for the mode $p \to \bar{\nu}K^+$ from dimension-five operators [66]. One possible way out is the cancellation mechanism for the reduction of proton decay arising from different Higgs triplet representations at the GUT scale [67]. This is equivalent to raising the value of the effective Higgs triplet mass. [68]. Specification of the GUT physics allows one to determine the effective Higgs triplet mass (see, e.g., Refs. [67,69]). Here, however, we do not commit to a specific GUT structure but rather consider $SU(5)$-like models in which, due to various Higgs representations that enter at the GUT scale, one has a number of Higgs triplets/antitriplets $H_i$, $\bar{H}_i$. Suppose we choose the basis in which only $H_1$, $\bar{H}_1$ couple to matter, i.e., one has couplings of the type [68] $\bar{H}_1 J + \bar{K}H_1 + \bar{H}_i M_{ij} H_j$, where $J$ and $\bar{K}$ are bilinear in matter fields and $M_{ij}$ is the superheavy Higgs mass matrix. Many grand unified models automatically lead to such a possibility [70,71]. Specifically in models of the type discussed in Ref. [70], one has only one light doublet and several Higgs triplets/antitriplets. On eliminating the superheavy fields, one finds that the effective proton decay operator is of the form $-\bar{K}(M'_{H_3})^{-1}J$ where $M'_{H_3} = (M_{11}^{-1})^{-1}$. This allows $M'_{H_3}$ to be much larger than the GUT scale. In the analysis here, we will use the effective mass $M_{H_3}^{\rm eff} = M'_{H_3}/A_L A_S$, and we consider three cases $M_{H_3}^{\rm eff}/M_G = 10$, 25, 50 for analysis in this work.

In Fig. 2 we exhibit the dependence of the proton lifetime for the decay mode $p \to \bar{\nu}K^+$ as a function of the Higgs boson mass under the constraints discussed in the caption of Fig. 2. The curves show a very sharp dependence of the proton lifetime on the Higgs boson mass, which increases by up to 2 orders of magnitude with a shift in the mass of the Higgs boson in the range of 5–10 GeV. In Fig. 3 we exhibit the proton lifetime for the decay mode $p \to \bar{\nu}K^+$ as a function of $m_0$ for the three values of $M_{H_3}^{\rm eff}$ when all the parameters in the model are allowed to vary consistent with the radiative electroweak symmetry breaking constraints and the experimental constraints including

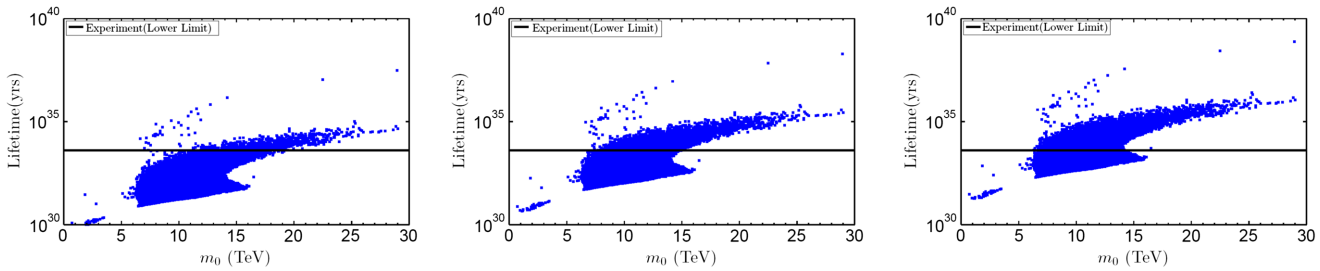


FIG. 3 (color online). An exhibition of the partial lifetime for the decay mode $p \to \bar{\nu}K^+$ given by blue squares as a function of $m_0$ over the parameter space of the supergravity model with universal boundary conditions over the allowed ranges consistent with all the experimental constraints. Left panel: The case when $M_{H_3}^{\rm eff}/M_G = 10$. Middle panel: Same as the left panel except for the case $M_{H_3}^{\rm eff}/M_G = 25$. Right panel: Same as the left panel except for the case $M_{H_3}^{\rm eff}/M_G = 50$. The current experimental lower limit for this mode is given by the horizontal black line. The analysis given here is consistent with the Higgs boson mass within a $2\sigma$ range.

those from the LHC and the Planck experiment. One finds that the parameters compatible with all the constraints clearly prefer values of $m_0$ in the several TeV region.

## IV. NUSUGRA: FOCAL CURVES AND FOCAL SURFACES

In Sec. II a classification of radiative breaking of the electroweak symmetry is given in terms of the branches on which the allowed parameter space of mSUGRA resides. Here, we extend the analysis to NuSUGRA and classify the allowed parameter space under the constraints of radiative breaking of the electroweak symmetry and all the experimental constraints, i.e., we discuss the composition of the parameter space in terms of the HB, EB, and FP. We will also discuss the sensitivity of the proton decay lifetime for the mode $p \to \bar{\nu} K^+$ for the NuSUGRA case. For specificity, we define the gaugino masses at the grand unification scale by $m_i$ where $m_i = m_{1/2}(1+\delta_i)$, $i = 1, 2, 3$ and where $\delta_i$ define the nonuniversalities in the $U(1)$, $SU(2)_L$, $SU(3)_C$ sectors. It is shown in Appendix B that in this case the radiative electroweak symmetry breaking equation, Eq. (1), for the universal soft breaking case is replaced by

$$\mu^2 + \frac{1}{2}M_Z^2 = C_1 m_0^2 + C_2 A_0^2 + \tilde{C}_3^{ij} m_i m_j + \tilde{C}_4^i m_i A_0 + \Delta\mu^2, \tag{16}$$

where $C_1$ and $C_2$ are as defined by Eq. (2) while $\tilde{C}_3^{ij}$ and $\tilde{C}_4^i$ are given by

$$\tilde{C}_3^{ij} = \frac{(M_{m_{H_1}})_{ij} - \tan^2\beta (M_{\tilde{e}})_{ij}}{\tan^2\beta - 1}, \qquad \tilde{C}_4^i = -\frac{\tan^2\beta}{\tan^2\beta - 1}(M_{\tilde{f}})_i. \tag{17}$$

Here, $M_{m_{H_1}}$, $M_{\tilde{e}}$, and $M_{\tilde{f}}$ are defined in Appendix B. $\tilde{C}_3$ and $\tilde{C}_4$ in Eq. (17) reduce to the universal case when $m_i = m_{1/2}$, and in this case one has $C_3 = \sum_{i,j=1,2,3}\tilde{C}_3^{ij}$ and $C_4 = \sum_{i=1,2,3}\tilde{C}_4^i$. In Fig. 9 we display the dependence of $\tilde{C}'s$ on the RG scale $Q$. Here, one finds that in addition to $C_1$, $\tilde{C}_3^{11}$ and $\tilde{C}_3^{22}$ assume negative values, which gives the possibility of new focal curves. We discuss these possibilities in further detail below.

To examine the focal curves and focal surfaces for NuSUGRA, it is useful to define

$$C_3^G m_{1/2}^2 = \tilde{C}_3^{ij} m_i m_j, \qquad C_4^G m_{1/2} = \tilde{C}_4^i m_i. \tag{18}$$

Further, in order to classify various regions of the radiative electroweak symmetry breaking (REWSB) for the NuSUGRA case, it useful to write the REWSB constraint Eq. (16) in the form

$$\mu^2 + \frac{1}{2}M_Z^2 = C_1 m_0^2 + C_2 \bar{A}_0^2 + C_3^{(i)} \bar{m}_i^2, \tag{19}$$

with

$$\bar{A}_0^2 = \left(A_0 + \sum_{i=1}^3 a_i m_i\right)^2, \qquad \bar{m}_i = \sum_{j=1}^3 a_{ij} m_j, \tag{20}$$

where $a_i$ and $a_{ij}$ are coefficients of linear combinations and they are functions of $C_2$, $\tilde{C}_3^{ij}$, and $\tilde{C}_4^i$.

A display of the renormalization group evolution of the $C_i$ is given in Fig. 9 in Appendix B. Here, we find that in addition to $C_1$, the elements $\tilde{C}_3^{11}$ and $\tilde{C}_3^{22}$ are negative, which allows for the possibility of new focal curves and focal sufaces over the ones discussed in Sec. II. Using the results of Appendixes A and B, one finds that four types of focal curves arise for the NuSUGRA case, FC1-FC4, which are listed in Table II. FC1 is defined similar to the case for mSUGRA. FC2 has three variations: These are HB/FC2$^{01}$, where $C_1 > 0$, $\tilde{C}_3^{11} < 0$ and $m_0$ and $m_1$ get large while $A_0$, $m_2$, $m_3$ and $\tan\beta$ remain fixed; HB/FC2$^{02}$, where $C_1 > 0$, $\tilde{C}_3^{22} < 0$ and $m_0$ and $m_2$ get large while $A_0$, $m_1$, $m_3$ and $\tan\beta$ remain fixed; and HB/FC2$^{03}$, where $C_1 < 0$, $\tilde{C}_3^{33} > 0$ and $m_0$ and $m_3$ get large while $A_0$, $m_1$, $m_2$ and $\tan\beta$ remain fixed. It is convenient to use the parametrization of Eq. (18) to exhibit the effect of nonuniversality on focal curves FC2. Thus, here, one finds that the asymptotic value of $m_{1/2}/m_0$ for fixed $\mu$ as $A_0$ gets large is affected by nonuniversality, i.e., one gets

$$\frac{m_{1/2}}{m_0} \to \sqrt{\frac{|C_1|}{C_3^G}}. \tag{21}$$

An illustration of the dependence of $m_{1/2}/m_0$ on nonuniversalities for FC2 will be exhibited shortly.

The focal curves FC3 arise when two of the gaugino masses get large while other soft parameters remain fixed.

TABLE II. Classification of focal curves in NuSUGRA models. Here, one has the possibility of several focal curves. The focal curve HB/FC1 is defined similarly to the mSUGRA case except that $m_1$, $m_2$, $m_3$ are all kept fixed. As in mSUGRA here, too, $m_0$ and $A_0$ can get large while $\mu$ remains fixed. The focal curve HB/FC2 splits into three subcases because of the gaugino nonuniversalities. Thus, the case HB/FC2$^{01}$ corresponds to the case when $A_0$, $m_2$, $m_3$ are kept fixed while $m_0$ and $m_1$ can get large. The focal curves HB/FC2$^{02}$ and HB/FC$^{03}$ are similarly defined. For the NuSUGRA case, four new types of focal curves arise. These are HB/FC3$^{13}$, HB/FC3$^{23}$, HB/FC4$^1$, and HB/FC4$^2$. Their definitions are obvious from the table.

| Focal curve | Large soft parameters | Small soft parameters |
|---|---|---|
| HB/FC1 | $m_0 - A_0$ | $m_1, m_2, m_3$ |
| HB/FC2$^{01}$ | $m_0 - m_1$ | $A_0, m_2, m_3$ |
| HB/FC2$^{02}$ | $m_0 - m_2$ | $A_0, m_1, m_3$ |
| HB/FC2$^{03}$ | $m_0 - m_3$ | $A_0, m_1, m_2$ |
| HB/FC3$^{13}$ | $m_1 - m_3$ | $m_0, A_0, m_2$ |
| HB/FC3$^{23}$ | $m_2 - m_3$ | $m_0, A_0, m_1$ |
| HB/FC4$^1$ | $A_0 - m_1$ | $m_0, m_2, m_3$ |
| HB/FC4$^2$ | $A_0 - m_2$ | $m_0, m_1, m_3$ |

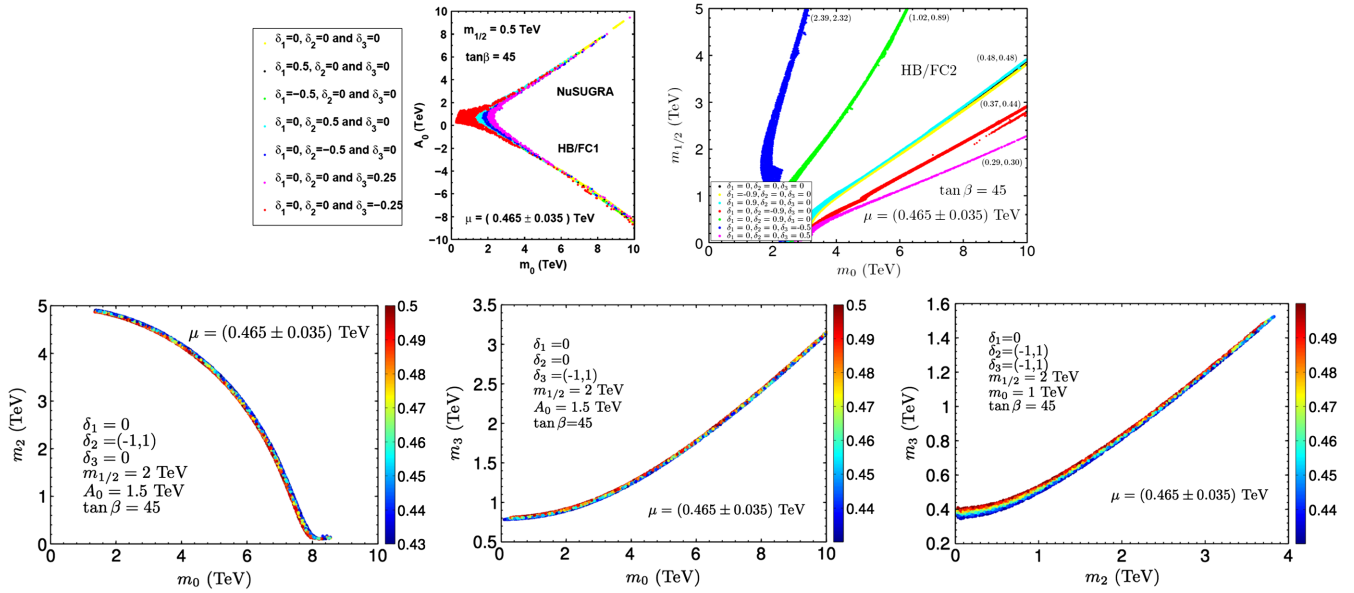


FIG. 4 (color online). Top left panel: Exhibition of the focal curve HB/FC1 of Table II with nonuniversalities in the gaugino sector. Here and in the right panel, $\tan\beta = 45$ with $\mu = (0.465 \pm 0.035)$ TeV. The plot shows that nonuniversalities in the gaugino sector do not affect the asymptotic behavior of $A_0/m_0$, which is unchanged from the mSUGRA case. Top right panel: Exhibition of the effect of nonuniversalities on focal curves FC2. The analysis shows that the nonuniversalites have a very significant effect of FC2-type focal curves. The asymptotic form of the FC2 curves with nonuniversalities fits well with the result of Eq. (21). Bottom panels show the three varieties of FC2 curves. Bottom left panel: An exhibition of the focal curve HB/FC2$^{03}$ in the $m_0 - m_3$ plane when $m_1 = m_3 = m_{1/2} = 2$ TeV and $A_0 = 1.5$ TeV. Bottom middle panel: A display of the focal curve HB/FC2$^{02}$ in the $m_0 - m_2$ plane when $m_1 = m_3 = m_{1/2} = 2$ TeV and $A_0 = 1.5$ TeV. Bottom right panel: An exhibition of the focal curve HB/FC3$^{23}$ in the $m_2 - m_3$ plane when $m_1 = m_{1/2} = 2$ TeV, $m_0 = 1$ TeV and $|A_0/m_0| < 0.1$. The model points are colored by the $\mu$ value in units of TeV.

There are two possibilities here. The first one is HB/FC3$^{13}$, where $m_1$ and $m_3$ get large while $A_0$, $m_0$, $m_2$, and $\tan\beta$ remain fixed. This can happen when $C_1 > 0$ but $\tilde{C}_3^{11}$ is negative. The second possibility is HB/FC3$^{23}$, where $m_2$ and $m_3$ get large while $A_0$, $m_0$, $m_1$ and $\tan\beta$ remain fixed. This can happen when $C_1 > 0$ but $\tilde{C}_3^{22}$ is negative. The focal curves FC4 arise when $A_0$ and one of the gaugino masses get large while the remaining soft parameters remain fixed. There are two possibilities here. The first one is HB/FC4$^1$, where $A_0$ and $m_1$ get large while $m_0$, $m_2$, $m_3$, and $\tan\beta$ remain fixed. This can happen since $C_2 > 0$ but $\tilde{C}_3^{11}$ is negative. The second possibility is HB/FC4$^2$, where $A_0$ and $m_2$ get large while $m_0$, $m_1$, $m_3$, and $\tan\beta$ remain fixed. This can happen when $C_2 > 0$ but $\tilde{C}_3^{22}$ is negative. We note that HB/FC3$^{12}$ does not materialize since $\tilde{C}_3^{11}$ and $\tilde{C}_3^{22}$ are both negative. Similarly, HB/FC4$^3$ does not occur since $C_2$ and $\tilde{C}_3^{33}$ are both positive. Further, while in principle HB/FC2$^{03}$ can occur when $C_1 < 0$ and $\tilde{C}_3^{33}$ is positive, the numerical sizes do not favor the appearance of this branch. Thus, as shown in the figures in Appendix B, $\tilde{C}_3^{aa}$ satisfy $|\tilde{C}_3^{11}| \ll |\tilde{C}_3^{22}| \ll |\tilde{C}_3^{33}|$, where each step is roughly a factor of 10. Thus, in practice the focal curve HB/FC2$^{03}$ does not materialize. Further, for any value of $\tan\beta$, the coefficient $C_1$ begins positive, and for $\tan\beta \lesssim 5$ it never becomes negative (for $Q \lesssim 10$ TeV). Because of the above, additional possibilities such as HB/FC3$^{12}$, etc., are not realized.

For NuSUGRA we give a numerical illustration of some of the focal curves in Fig. 4. The left panel of the top row in Fig. 4 gives an analysis of the FC1 in the $m_0 - A_0$ plane.

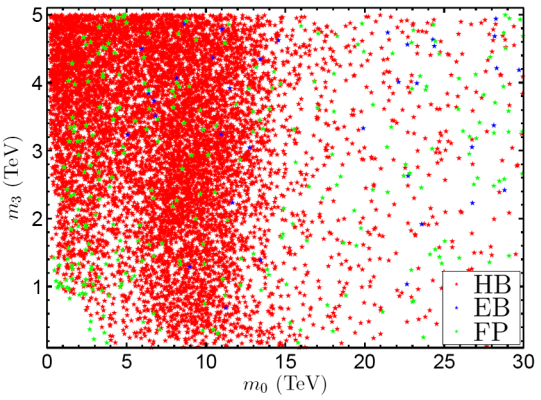


FIG. 5 (color online). Exhibition of HB (red), EB (blue), and FP (green) parameter points for NuSUGRA using the inputs given in Sec. II. All parameter points satisfy the general constraints along with a $2\sigma$ constraint on the Higgs boson mass. As in the supergravity unified models with universal boundary conditions, here, too, one finds that most of the allowed parameter space lies on the HB branch while EB and FP regions are highly depleted.

Here, one finds that $m_0$ and $A_0$ can get as large as 10 TeV while $\mu$ lies in the range $(0.465 \pm 0.035)$ TeV when $\tan\beta = 45$ and $m_{1/2} = 0.5$ TeV. We note that the ratio $A_0/m_0$ asymptotes to the same value irrespective of the nonuniversalities. A similar analysis for FC2 is given in the right panel of Fig. 4 in the $m_0 - m_{1/2}$ plane for $\tan\beta = 45$. Again, a variety of nonuniversalities are discussed. One finds that while $m_0$ and $m_{1/2}$ can get very large, i.e., as large as 10 TeV for $m_0$ and 5 TeV for $m_{1/2}$, one still has a small $\mu$, i.e., a $\mu$ range $(0.465 \pm 0.035)$ TeV. An analysis for FC3 is given in the three panels of the bottom row in Fig. 4. The left panel gives a display of the focal curve $FC3^{02}$ in the $m_0 - m_2$ plane for the case when $\tan\beta = 45$, $A_0 = 1.5$ TeV, $m_{1/2} = 2$ TeV, and $\delta_1 = 0 = \delta_3$, and $\delta_2$ lies in the range $(-1, 1)$. One finds that $\mu$ lies in the narrow range $(0.465 \pm 0.035)$ TeV. A very similar analysis in the $m_0 - m_3$ plane is given in the middle panel in Fig. 4, where $\delta_1 = 0 = \delta_2$ and $\delta_3$ lies in the range $(-1, 1)$ while all other parameters are as in the left panel. This is the focal curve $FC3^{03}$. Finally, the right panel gives an analysis of the $FC3^{23}$ in the $m_2 - m_3$ plane for the case when $m_0 = 1$ TeV, $m_{1/2} = 2$ TeV, $\tan\beta = 45$, and $\delta_0 = 0$, $\delta_2 = (-1, 1)$, and $\delta_3 = (-1, 1)$. Here, again, one finds that $\mu$ lies in the range $(0.465 \pm 0.0350)$ TeV while $m_2$, $m_3$ get large. From a convolution of the focal curves, one can generate focal surfaces on which more than two soft parameters can vary while $\mu$ remains fixed.

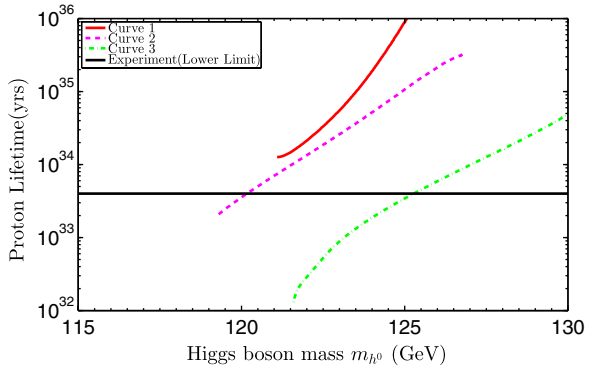


FIG. 6 (color online). An exhibition of the dependence of the proton lifetime for the decay mode $p \to \bar{\nu}K^+$ as a function of the Higgs boson mass for NuSUGRA. Parameters for the curves labelled 1–3 in the legend are as follows. Curve 1: $m_1 = 4230$ GeV, $m_2 = 843$ GeV, $m_3 = 3285$ GeV, $A_0 = -27545$ GeV, and $\tan\beta = 5.3$ while $m_0$ varies and $M_{H_3}^{\rm eff}/M_G = 50$ here and for other curves. Curve 2: $m_1 = 4794$ GeV, $m_2 = 3837$ GeV, $m_3 = 3856$ GeV, $A_0/m_0 = 0.842$, and $\tan\beta = 7.0$ while $m_0$ and $A_0$ vary. Curve 3: $m_1 = 3894$ GeV, $m_2 = 1056$ GeV, $m_3 = 2345$ GeV, $A_0/m_0 = 2.199$, and $\tan\beta = 55.2$ while $m_0$ and $A_0$ vary. As for the case of the supergravity unified models with universal boundary conditions, here, too, one finds that the proton lifetime is a very sensitive function of the Higgs boson mass.

In Fig. 5 we display the nature of radiative breaking of the electroweak symmetry for all the model points within the allowed ranges of the parameter space for NuSUGRA. The points in red are those that lie on the HB, the points in blue lie on the EB, and the points in green lie in the FP region as defined by Eqs. (6) and (7). As in the mSUGRA case, here, too, one finds that most of the parameter points lie on the HB, and only a small fraction lie on the EB and FP. In Fig. 6 we give an analysis of the sensitivity of the proton lifetime to the Higgs boson mass for NuSUGRA. As in the mSUGRA case, here, too, one finds that the proton lifetime is very sensitive to the Higgs boson mass with the proton lifetime changing by over 2 orders of magnitude with a shift in the Higgs boson mass in the range of 5–10 GeV. In Fig. 7 an analysis of the proton lifetime for the mode $p \to \bar{\nu}K^+$ is given over the allowed parameter space of NuSUGRA within the assumed limits. The figure shows the dispersion in the proton lifetime as all the parameter points are varied but does show the general trend that the $p \to \bar{\nu}K^+$ lifetime increases with a larger SUSY scale.

## V. NATURALNESS

The criteria used for quantifying what is naturalness are rather subjective, and various variants abound see, e.g., Refs. [16,24,72–83]. Here, we discuss the fine-tuning within a GUT framework including both radiative breaking

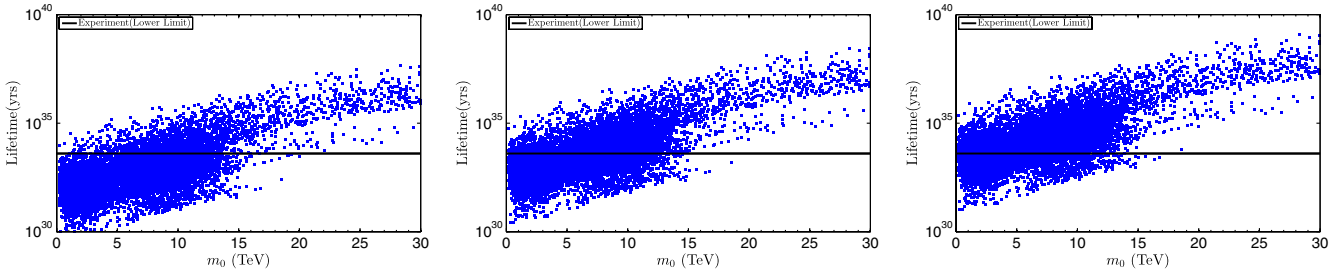


FIG. 7 (color online). Left panel: The proton lifetime shown as blue squares over the allowed parameter space in NuSUGRA models, which pass the general constraints along with a $2\sigma$ constraint for the Higgs boson mass as discussed in the text when $M_{H_3}^{\rm eff}/M_G = 10$. Middle panel: Same as the left panel except that $M_{H_3}^{\rm eff}/M_G = 25$. Right panel: Same as the left panel except that $M_{H_3}^{\rm eff}/M_G = 50$. The current experimental lower limit on the proton lifetime is shown as a black horizontal line. The analysis given here is consistent with the Higgs boson mass within a $2\sigma$ range.

of the electroweak symmetry and proton stability. First, we discuss fine-tuning for radiative breaking of the electroweak symmetry, which is governed by the breaking condition Eq. (1). If one views $M_Z^2$ as arising from the cancellation between the $\mu^2$ term and the remainder on the right-hand side, it leads to a fine-tuning [24]:

$$F \simeq \frac{4\mu^2}{M_Z^2}. \tag{22}$$

An alternate criteria for fine-tuning is given by the condition [72] $F'_a = (a/f(a))f'(a)$, where $a$ is the sensitive parameter on which the function $f(a)$ depends. Using $f(a) = M_Z^2$ and the sensitive parameter as $m_{H_u}^2$, one finds another fine-tuning measure:

$$F' \simeq \frac{2|m_{H_u}^2|}{M_Z^2}. \tag{23}$$

We will use both $F$ and $F'$ in the analysis for comparison. For proton decay we will use a measure of fine-tuning defined by

$$F_{pd} = \frac{4 \times 10^{33}\ \text{yr}}{\tau(p \to \bar{\nu}K^+)\text{yr}}. \tag{24}$$

This measure gives the amount of fine-tuning needed in the theory parameters to enhance the lifetime so that the theoretical prediction is brought just above the current experimental lower limit. If we use the very crude

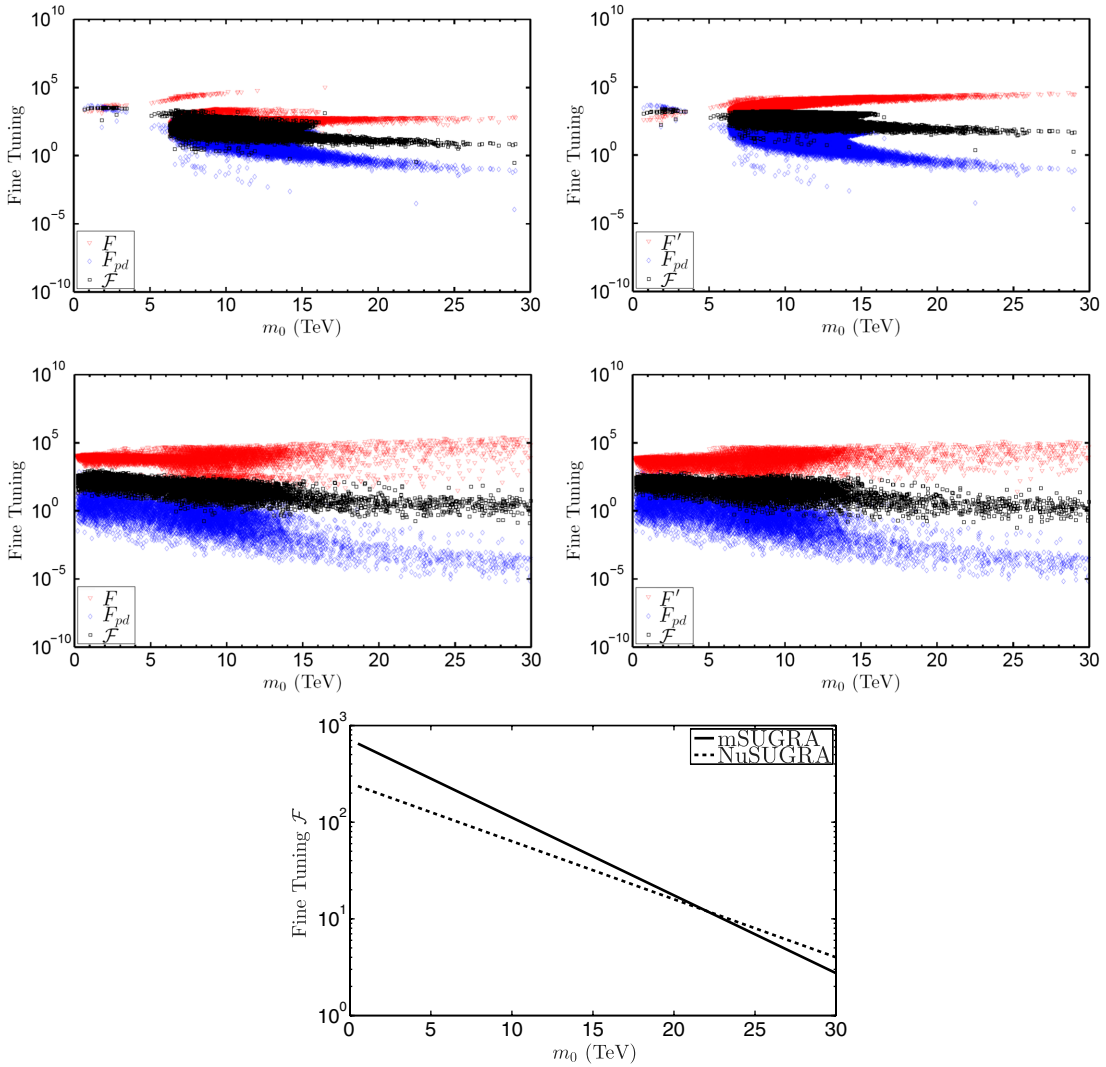


FIG. 8 (color online). A display of the fine-tuning as defined by Eqs. (22)–(25) vs the scalar mass $m_0$ when $M_{H_3}^{\text{eff}}/M_G = 50$. The upper two panels are for mSUGRA, and the middle two panels are for the NuSUGRA case. The left panels are when we use the fine-tuning of Eq. (22), and the right panels are when we use the fine-tuning of Eq. (23) for the electroweak sector. The red points are the fine-tuning values for the REWSB sector, the blue points for $\tau(p \to \bar{\nu}K^+)$, and the black points are the averages of the red and the blue points. In the bottom panel, the combined fine-tuning as a function of $m_0$ is given for mSUGRA (sold line) and for NuSUGRA (dashed line). Here, we have taken the average of the left and right panels and drawn smooth curves showing the rapid decrease of the fine-tunings as $m_0$ increases.

approximation on the proton lifetime, i.e., $\tau(p \to \bar{\nu}K^+) \simeq C \cdot (m_{\tilde{\chi}^\pm}/m_{\tilde{q}}^2 M_{H_3}^{\rm eff})^{-2}$, and use $m_{\tilde{q}}^2$ or $m_{\chi^\pm}$ as the sensitive parameters, we have $F'_{m_{\chi^\pm}} = F'_{m_{\tilde{q}}^2} = 2F_{pd}$. Thus, the two ways of defining the fine-tuning differ only by a small numerical factor. It is also useful to define a composite fine-tuning by the geometric mean of the individual ones, i.e.,

$$\mathcal{F} = \left(\prod_{i=i}^{n} F_i\right)^{\frac{1}{n}}. \tag{25}$$

Here, our view point is similar to that of Ref. [82] (for a related work, see Ref. [84]). For our case $n = 2$ consisting of the fine-tuning in the radiative electroweak symmetry breaking sector and the fine-tuning needed to control proton decay from dimension-five operators. An analysis of the fine-tunings as a function of $m_0$ is given in Fig. 8, where the upper panels give the analysis for the case of mSUGRA, the middle panels give the analysis for NuSUGRA, the left panels give the analysis using Eq. (22), and the right panels give the analysis using Eq. (23). The red points are the fine-tunings for radiative electroweak symmetry breaking. The blue points give the fine-tuning needed in the theory prediction of $\tau(p \to \bar{\nu}K^+)$ to bring the lifetime prediction just above the experimental lower limit, and the black points correspond to the composite fine-tuning as defined by Eq. (25). One finds that typically there is a preference for larger values of $m_0$ for the combined fine-tuning including fine-tuning from the electroweak sector and the fine -tuning needed from proton stability. This result is more explicitly exhibited in the bottom panel of Fig. 8, which shows fine-tuning prefers regions of larger $m_0$ when the electroweak symmetry breaking and proton stability criteria are combined. A similar conclusion was arrived at in the work of Ref. [82], which combined the electroweak symmetry breaking, FCNC, and *CP*-violation criteria.

## VI. CONCLUSIONS

The high mass of the Higgs boson discovered recently requires a large loop correction to its mass, which points to the possibility that the overall weak scale of supersymmetry may lie in the several TeV region and could even be as large as tens of TeV. If the scalar masses are that large, they would help resolve one of the serious problems of supersymmetric grand unification related to proton decay. Thus, proton decay from lepton- and baryon-number violating dimension-five operators often leads to proton lifetimes which fall below the current experimental limits. In this work we show that the proton lifetime is a very sensitive function of the Higgs boson mass in a unified theory. Thus, a few GeV upward shift in the Higgs boson can result in orders of magnitude suppression of the proton decay from baryon- and lepton-number violating dimension-five operators and a corresponding enhancement of the proton lifetime. The analysis is first done for the mSUGRA model and then extended to NuSUGRA. Here, we also analyze the allowed parameter space in terms of on which branch of the radiative breaking of the electroweak symmetry the parameters lie, i.e., whether on the ellipsoidal branch, the hyperbolic branch, or the focal point region. The analysis presented in this work shows that, under the current experimental constraints including those from the large electron-positron collider, Tevatron, LHC, FCNC, and Planck data [85], one finds that most of the parameter points of mSUGRA and of NuSUGRA models lie on the hyperbolic branch with only a very small fraction lying on the ellipsoidal branch or in the focal point region. We also discuss issues of naturalness and fine-tuning and show that the composite fine-tuning including fine-tuning from the electroweak sector and from the stability of the proton points to high scalar masses. However, some of the gauginos can be light with their masses mostly limited by their lower experimental limits. These include the light chargino, the lightest neutralino, the second-lightest neutralino, and the gluino. These should be accessible with increased energy and luminosity at the next round of experiment at the LHC. Regarding proton decay discovery of the supersymmetric mode, $p \to \bar{\nu}K^+$ is overdue, and this mode continues to be the most likely candidate to be discovered first in the next generation of proton decay experiments.

## ACKNOWLEDGMENTS

Collaboration in the initial stages of this work with Sujeet Akula and Gregory Peim is acknowledged. M. L. also thanks them for help with numerical analysis in this work. This research is supported in part by the U.S. National Science Foundation (NSF) Grants No. PHY-0757959 and No. PHY-070467 and DOE NERSC Grant No. DE-AC02-05CH11231.

## APPENDIX A: THE RELATION OF $C_1(Q)$ TO $m_{H_2}$

Here, we establish the relation between the $C_1(Q)$ and $m_{H_2}$. The RG evolution connects $m_{H_2}$, and on the third-generation masses $m_U$ and $m_Q$, and one has

$$\frac{d}{dt}\begin{bmatrix} m_{H_2}^2 \\ m_U^2 \\ m_Q^2 \end{bmatrix} = -Y_t \begin{bmatrix} 3 & 3 & 3 \\ 2 & 2 & 2 \\ 1 & 1 & 1 \end{bmatrix} \begin{bmatrix} m_{H_2}^2 \\ m_U^2 \\ m_Q^2 \end{bmatrix} - Y_t A_t^2 \begin{bmatrix} 3 \\ 2 \\ 1 \end{bmatrix} + \begin{bmatrix} 3\tilde{\alpha}_2 m_2^2 + \tilde{\alpha}_1 m_1^2 \\ \frac{16}{3}\tilde{\alpha}_3 m_3^2 + \frac{16}{9}\tilde{\alpha}_1 m_1^2 \\ \frac{16}{3}\tilde{\alpha}_3 m_3^2 + 3\tilde{\alpha}_2 m_2^2 + \frac{1}{9}\tilde{\alpha}_1 m_1^2 \end{bmatrix}. \tag{A1}$$

Here, $Y_t = h_t^2/(4\pi^2)$ where $h_t$ is the top Yukawa coupling and $A_t$ is the trilinear coupling in the top sector. The above equations with universal boundary conditions at the GUT scale allow a homogeneous solution satisfying [31]

$$\begin{bmatrix} \delta m_{H_2}^2 \\ \delta m_U^2 \\ \delta m_Q^2 \end{bmatrix} = \frac{m_0^2}{2} \begin{bmatrix} 3J(t) - 1 \\ 2J(t) \\ J(t) + 1 \end{bmatrix}, \tag{A2}$$

where $J$ is an integration factor defined by

$$J(t) \equiv \exp\left[-6 \int_0^t Y_t(t')dt'\right]. \tag{A3}$$

As $Q \to M_G$, one has $J(t) \to 1$, and the universality of the masses is recovered at the GUT scale. In Ref. [32] a connection was established between $C_1(Q)$ and $\delta m_{H_2}$, which we now illustrate. Thus, $Y(t)$ at the one-loop level satisfies the equation

$$\frac{dY_t}{dt} = \left(\frac{16}{3}\tilde{\alpha}_3 + 3\tilde{\alpha}_3 + \frac{13}{9}\tilde{\alpha}_1\right)Y_t - 6Y_t^2, \tag{A4}$$

and one finds

$$Y_t(t) = \frac{Y(0)E(t)}{1 + 6Y(0)F(t)}, \tag{A5}$$

where $F(t)$ and $E(t)$ are defined after Eq. (4). It is then easy to see that $J(t) = D_0(t)$, where $D_0(t)$ is defined by Eq. (4). Thus, $\delta m_{H_2}^2$ takes the form

$$\delta \bar{m}_{H_2}^2 \equiv \frac{\delta m_{H_2}^2}{m_0^2} = \frac{1}{2}(3D_0 - 1), \tag{A6}$$

and $C_1$ can be expressed in terms of $\delta \bar{m}_{H_2}^2$

$$C_1 = \frac{1}{\tan^2\beta - 1}(1 - \delta \bar{m}_{H_2}^2 \tan^2\beta) \simeq -\delta \bar{m}_{H_2}^2. \tag{A7}$$

$C_1 = 0$ was defined as the focal point in Ref. [32]. At the focal point, $\mu^2$ essentially becomes independent of $m_0$. For $\tan\beta \gg 1$, $C_1 \simeq -\delta \bar{m}_{H_2}^2$, and the vanishing of $C_1$ implies the vanishing of $\delta \bar{m}_{H_2}^2$ which is defined to be the focus point. Thus, the focal point defined by $C_1 = 0$ is just the boundary point between the EB defined by $C_1 > 0$ and HB defined by $C_1 < 0$. For the NuSUGRA models, all solutions in which some of the soft parameters can get large while $\mu^2$ remains fixed lie on the HB. This can happen when some of the $C_i$ other than $C_1$ turn negative, as discussed in Appendix B below.

## APPENDIX B: ANALYSIS OF $C_i'$s FOR MODELS WITH NONUNIVERSALITIES IN THE GAUGINO SECTOR

The presence of nonuniversalities in the gaugino sector affects the coefficients $C_i$, and in this appendix we give a computation for these by inclusion of nonuniversalities in the $SU(3)_C$, $SU(2)_L$, and $U(1)$ gaugino sectors. We begin with the radiative electroweak symmetry breaking with the inclusion of nonuniversalities in the gaugino sector. We have

$$\mu^2 = \frac{(m_{H_1}^2 - m_{H_2}^2 \tan\beta^2)}{(\tan\beta^2 - 1)} - \frac{1}{2}M_Z^2 + \Delta\mu^2, \tag{B1}$$

with

$$m_{H_1}^2 = m_0^2 + \left(\frac{3}{10}\tilde{f}_1 + \frac{3}{2}\tilde{f}_2\right), \tag{B2}$$

$$m_{H_2}^2 = \tilde{e}(t) + A_0\tilde{f}(t) + m_0^2 h(t) - A_0^2 k(t), \tag{B3}$$

and $\tilde{f}_i(t)$ is defined by $\tilde{f}_i(t) = Z_i^f m_i^2$, where

$$Z_i^f = \frac{1}{\beta_i}\left(1 - \frac{1}{(1 + \beta_i t)^2}\right)\tilde{\alpha}_i(0). \tag{B4}$$

It is useful to introduce a column vector $\vec{m}^T = (m_1, m_2, m_3)$ and a matrix $M_{m_{H_1}}$ such that $m_{H_1}^2 = \vec{m}^{\mathsf{T}} \cdot M_{m_{H_1}} \cdot \vec{m} = (M_{m_{H_1}})_{ij} m_i m_j$ where $M_{H_1}$ is given by

$$M_{m_{H_1}} = \begin{pmatrix} \frac{3}{10}Z_1^f & 0 & 0 \\ 0 & \frac{3}{2}Z_2^f & 0 \\ 0 & 0 & 0 \end{pmatrix}. \tag{B5}$$

Thus, we have

$$m_{H_1}^2 = m_0^2 + (M_{m_{H_1}})_{ij} m_i m_j. \tag{B6}$$

The above exhibits the gaugino mass dependence of $m_{H_1}^2$ explicitly. Now let us look at $m_{H_2}^2$ given by Eq. (B3) and write it in a form which exhibits the gaugino mass dependence explicitly. Now $m_{H_1}^2$ contains the functions $\tilde{e}(t)$ and $\tilde{f}(t)$, which are given as

$$\begin{aligned} \tilde{e} &= \frac{3}{2}\left[\frac{\tilde{G}_1 + Y_0\tilde{G}_2}{D(t)} + \frac{(\tilde{H}_2 + 6Y_0\tilde{H}_4)^2}{3D(t)^2} + \tilde{H}_8\right], \\ \tilde{f} &= -\frac{6Y_0\tilde{H}_3(t)}{D(t)^2}, \end{aligned} \tag{B7}$$

where $\tilde{H}_i(t)$ are defined by

$$\begin{aligned} \tilde{H}_2 &= \frac{13}{15}\tilde{h}_1(t) + 3\tilde{h}_2(t) + \frac{16}{3}\tilde{h}_3(t), \\ \tilde{H}_3 &= \int_0^t E(t')\tilde{H}_2(t')dt', \end{aligned} \tag{B8}$$

$$\begin{aligned} \tilde{H}_4 &= F(t)\tilde{H}_2(t) - \tilde{H}_3(t), \\ \tilde{H}_5 &= \left(-\frac{22}{15}\tilde{f}_1(t) + 6\tilde{f}_2(t) - \frac{16}{3}\tilde{f}_3(t)\right), \end{aligned} \tag{B9}$$

$$\begin{aligned} \tilde{H}_6 &= \int_0^t E(t')\tilde{H}_2(t')^2 dt', \\ \tilde{H}_8 &= \tilde{\alpha}_G\left(-\frac{8}{3}\tilde{f}_1(t) + \tilde{f}_2(t) - \frac{1}{3}\tilde{f}_3(t)\right), \end{aligned} \tag{B10}$$

and $\tilde{h}_i$ are defined by $\tilde{h}_i \equiv Z_i^h m_i$ with

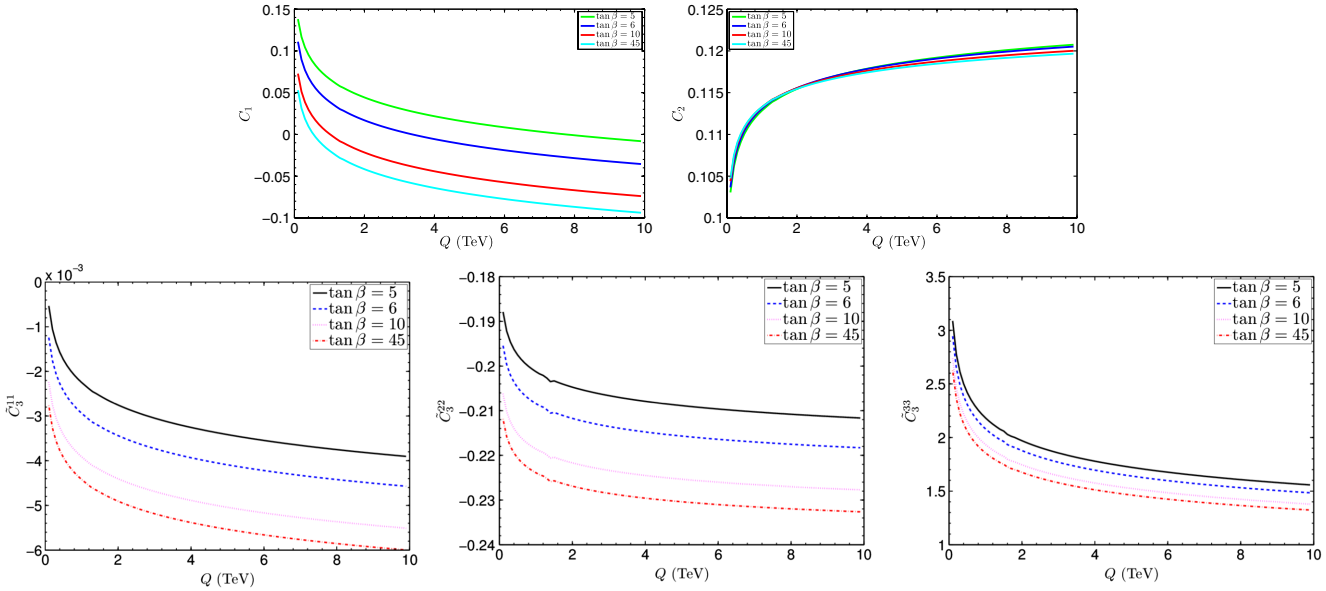


FIG. 9 (color online). The upper panels: RG evolution of $C_1(Q)$ and $C_2(Q)$ as a function of the renormalization group scale $Q$ at different tan $\beta$. Left panel: $C_1(Q)$ at tan $\beta = 5$, 6, 10, and 45. Right panel: $C_2(Q)$ at tan $\beta = 5$, 6, 10, and 45. It is seen that $C_1(Q)$ turns negative as the scale $Q$ increases while $C_2(Q)$ remains positive. It is also seen that $C_1(Q)$ is very sensitive to tan $\beta$ while $C_2$ is very insensitive to tan $\beta$. The lower panels: An exhibition of $\tilde{C}_3^{ii}$ at different tan $\beta$. Left panel: $\tilde{C}_3^{11}$ at tan $\beta = 5$, 6, 10, and 45. Middle panel: $\tilde{C}_3^{22}$ at tan $\beta = 5$, 6, 10, and 45. Right panel: $\tilde{C}_3^{33}$ at tan $\beta = 5$, 6, 10, and 45. It is seen that $\tilde{C}_3^{11}$ and $\tilde{C}_3^{22}$ are negative, which allows the possibility of new focal curves as discussed in the text.

$$Z_i^h = \frac{t}{1+\beta_i t}\tilde{\alpha}_i(0). \tag{B11}$$

$\tilde{H}_2(t)$ then takes the form

$$\tilde{H}_2 \equiv \vec{M}_{\tilde{H}_2}\cdot\vec{m}, \tag{B12}$$

where $\vec{M}_{\tilde{H}_2}$ is a row vector

$$\vec{M}_{\tilde{H}_2} = \left(\frac{13}{15}Z_1^h, 3Z_2^h, \frac{16}{3}Z_3^h\right). \tag{B13}$$

Similarly, we may write all the $M_{\tilde{H}_i}(t)$ in matrix or vector forms so that $\tilde{H}_3 = \vec{M}_{\tilde{H}_3}\cdot\vec{m}$, $\tilde{H}_4 = \vec{M}_{\tilde{H}_4}\cdot\vec{m}$, $\tilde{H}_5 = \vec{m}^{\mathsf{T}}\cdot M_{\tilde{H}_5}\cdot\vec{m}$, $\tilde{H}_6 = (\vec{M}_{\tilde{H}_8}\cdot\vec{m})^2$. $\tilde{H}_8 = \vec{m}^{\mathsf{T}}\cdot M_{\tilde{H}_8}\cdot\vec{m}$, where the matrices $\vec{M}_{\tilde{H}_3}$, etc., are given by

$$\begin{aligned}
\vec{M}_{\tilde{H}_3} &= \int_0^t E(t')\vec{M}_{\tilde{H}_2}(t')dt',\\
\vec{M}_{\tilde{H}_4} &= \vec{M}_{\tilde{H}_2}(t)\int_0^t E(t')dt' - \int_0^t \vec{M}_{\tilde{H}_2}(t')E(t')dt',\\
M_{\tilde{H}_5} &= \begin{pmatrix} -\frac{22}{15}Z_1^f & 0 & 0\\ 0 & 6Z_2^h & 0\\ 0 & 0 & -\frac{16}{3}Z_3^h\end{pmatrix},\\
M_{\tilde{H}_8} &= \begin{pmatrix} -\frac{1}{3}Z_1^f & 0 & 0\\ 0 & Z_2^h & 0\\ 0 & 0 & -\frac{8}{3}Z_3^h\end{pmatrix},
\end{aligned} \tag{B14}$$

$$M_{\tilde{H}_6} = \int_0^t (\vec{M}_{\tilde{H}_2}(t'))^{\mathsf{T}}(\vec{M}_{\tilde{H}_2}(t'))E(t')dt' \tag{B15}$$

Similarly, $\tilde{F}_i(t)$ defined by

$$\tilde{F}_2 = \frac{8}{15}\tilde{f}1 + \frac{8}{3}\tilde{f}2, \tag{B16}$$

$$\tilde{F}_3 = F(t)\tilde{F}_2(t) - \int_0^t E(t')\tilde{F}_2(t')dt', \tag{B17}$$

$$\tilde{F}_4 = \int_0^t E(t')\tilde{H}_5(t')dt' \tag{B18}$$

can also be written in matrix forms so that $\tilde{F}_2 \equiv (M_{\tilde{F}_2})_{ij}m_i m_j$, $\tilde{F}_3 \equiv (M_{\tilde{F}_3})_{ij}m_i m_j$, $\tilde{F}_4 \equiv (M_{\tilde{F}_4})_{ij}m_i m_j$, with $M_{\tilde{F}_i}$ defined by

$$M_{\tilde{F}_2}(t) = \begin{pmatrix} \frac{8}{15}Z_1^f & 0 & 0\\ 0 & 0 & 0\\ 0 & 0 & \frac{8}{3}Z_3^f\end{pmatrix}, \tag{B19}$$

$$\begin{aligned}
M_{\tilde{F}_3}(t) &= F(t)M_{\tilde{F}_2}(t) - \int_0^t E(t')M_{\tilde{F}_2}(t')dt',\\
M_{\tilde{F}_4}(t) &= \int_0^t E(t')M_{\tilde{H}_5}(t')dt'.
\end{aligned} \tag{B20}$$

We repeat the same procedure for functions $\tilde{G}_i$ defined by

$$\tilde{G}_1 = \tilde{F}_2(t) - \frac{1}{3}\tilde{H}_2(t)^2,$$
$$\tilde{G}_2 = 6\tilde{F}_3(t) - \tilde{F}_4(t) - 4\tilde{H}_2(t)\tilde{H}_4(t) + 2F(t)\tilde{H}_2(t)^2 - 2\tilde{H}_6(t), \quad \text{(B21)}$$

which could also been written as, $\tilde{G}_1(t) \equiv (M_{\tilde{G}_1})_{ij} m_i m_j$, $\tilde{G}_2(t) \equiv (M_{\tilde{G}_2})_{ij} m_i m_j$, with $M_{\tilde{G}_i}$ defined by

$$M_{\tilde{G}_1}(t) = M_{\tilde{F}_2} - \frac{1}{3}(\vec{M}_{\tilde{H}_2})^{\mathsf{T}} \cdot \vec{M}_{\tilde{H}_2}, \quad \text{(B22)}$$

$$M_{\tilde{G}_2}(t) = 6M_{\tilde{F}_3} - M_{\tilde{F}_4} - 4(\vec{M}_{\tilde{H}_2})^{\mathsf{T}} \cdot \vec{M}_{\tilde{H}_4} + 2F(\vec{M}_{\tilde{H}_2})^{\mathsf{T}} \cdot \vec{M}_{\tilde{H}_2} - 2M_{\tilde{H}_6}. \quad \text{(B23)}$$

We return now to $\tilde{e}(t)$ and $\tilde{f}(t)$ and write these in the matrix form so that $\tilde{e}(t) \equiv (M_{\tilde{e}})_{ij} m_i m_j$, and $\tilde{f}(t) \equiv (\vec{M}_{\tilde{f}})_i m_i$ with

$$M_{\tilde{e}} = \frac{3}{2D(t)^2}(3D(t)[M_{\tilde{G}_1} + Y_0 M_{\tilde{G}_2}] + \frac{1}{3}[\vec{M}_{\tilde{H}_2} + 6Y_0\vec{M}_{\tilde{H}_4}]^2 + D(t)^2 M_{\tilde{H}_8}),$$
$$\vec{M}_{\tilde{f}} = -\frac{6Y_0\vec{M}_{\tilde{H}_3}}{D(t)^2}. \quad \text{(B24)}$$

Using the above we can write $m_{H_2}^2$ in the form

$$m_{H_2}^2 = (M_{\tilde{e}})_{ij} m_i m_j + A_0(\vec{M}_{\tilde{f}})_i m_i + m_0^2 h(t) - A_0^2 k(t). \quad \text{(B25)}$$

Thus, using Eqs. (B6) and (B25) in Eq. (B1), we finally have the radiative electroweak symmetry breaking equation for nonuniversalities as given in Eq. (16).


[1] G. Aad *et al.* (ATLAS Collaboration), Phys. Lett. B **716**, 1 (2012).
[2] S. Chatrchyan *et al.* (CMS Collaboration), Phys. Lett. B **716**, 30 (2012).
[3] F. Englert and R. Brout, Phys. Rev. Lett. **13**, 321 (1964).
[4] P. W. Higgs, Phys. Rev. Lett. **13**, 508 (1964).
[5] G. Guralnik, C. Hagen, and T. Kibble, Phys. Rev. Lett. **13**, 585 (1964).
[6] S. Weinberg, Phys. Rev. Lett. **19**, 1264 (1967).
[7] A. Salam, *Elementary Paricle Theory* (Almqvist and Wiksells, Stockholm, 1968), p. 367.
[8] A. H. Chamseddine, R. L. Arnowitt, and P. Nath, Phys. Rev. Lett. **49**, 970 (1982); P. Nath, R. L. Arnowitt, and A. H. Chamseddine, Phys. Lett. **121B**, 33 (1983); for a review, see P. Nath, arXiv:hep-ph/0307123.
[9] P. Nath, R. L. Arnowitt, and A. H. Chamseddine, Nucl. Phys. **B227**, 121 (1983).
[10] L. J. Hall, J. D. Lykken, and S. Weinberg, Phys. Rev. D **27**, 2359 (1983).
[11] R. L. Arnowitt and P. Nath, Phys. Rev. Lett. **69**, 725 (1992).
[12] S. Akula, B. Altunkaynak, D. Feldman, P. Nath, and G. Peim, Phys. Rev. D **85**, 075001 (2012).
[13] S. Akula, P. Nath, and G. Peim, Phys. Lett. B **717**, 188 (2012).
[14] A. Arbey, M. Battaglia, A. Djouadi, and F. Mahmoudi, J. High Energy Phys. 09 (2012) 107.
[15] J. Ellis and K. A. Olive, Eur. Phys. J. C **72**, 2005 (2012).
[16] H. Baer, V. Barger, P. Huang, D. Mickelson, A. Mustafayev, and X. Tata, Phys. Rev. D **87**, 035017 (2013).
[17] P. Nath, Int. J. Mod. Phys. A **27**, 1230029 (2012).
[18] M. S. Carena and H. E. Haber, Prog. Part. Nucl. Phys. **50**, 63 (2003); A. Djouadi, Phys. Rep. **459**, 1 (2008).
[19] K. Babu, I. Gogoladze, M. U. Rehman, and Q. Shafi, Phys. Rev. D **78**, 055017 (2008).
[20] S. P. Martin, Phys. Rev. D **82**, 055019 (2010).
[21] W.-Z. Feng and P. Nath, Phys. Rev. D **87**, 075018 (2013).
[22] A. Joglekar, P. Schwaller, and C. E. M. Wagner, arXiv:1303.2969.
[23] L. Ibanez and G. Ross, C.R. Physique **8**, 1013 (2007).
[24] K. L. Chan, U. Chattopadhyay, and P. Nath, Phys. Rev. D **58**, 096004 (1998).
[25] U. Chattopadhyay, A. Corsetti, and P. Nath, Phys. Rev. D **68**, 035005 (2003).
[26] H. Baer, C. Balazs, A. Belyaev, T. Krupovnickas, and X. Tata, J. High Energy Phys. 06 (2003) 054.
[27] D. Feldman, G. Kane, E. Kuflik, and R. Lu, Phys. Lett. B **704**, 56 (2011).
[28] P. Nath and R. L. Arnowitt, Phys. Rev. D **56**, 2820 (1997); J. R. Ellis, K. A. Olive, and Y. Santoso, Phys. Lett. B **539**, 107 (2002).
[29] L. E. Ibanez, C. Lopez, and C. Munoz, Nucl. Phys. **B256**, 218 (1985); L. E. Ibanez and C. Lopez, Nucl. Phys. **B233**, 511 (1984).
[30] R. L. Arnowitt and P. Nath, Phys. Rev. D **46**, 3981 (1992).
[31] J. L. Feng, K. T. Matchev, and T. Moroi, Phys. Rev. Lett. **84**, 2322 (2000).
[32] S. Akula, M. Liu, P. Nath, and G. Peim, Phys. Lett. B **709**, 192 (2012).
[33] CMS Collaboration, Phys. Lett. B **698**, 196 (2011); CMS CollaborationPhys. Rev. Lett. **107**, 221804 (2011); CMS CollaborationReport No. CMS-PAS-SUS-11-005; CMS CollaborationReport No. CMS-PAS-SUS-11-006; CMS CollaborationReport No. CMS-PAS-SUS-11-013; CMS CollaborationReport No. CMS-PAS-SUS-11-015.
[34] ATLAS Collaboration, Phys. Rev. Lett. **106**, 131802 (2011).
[35] ATLAS Collaboration, Phys. Lett. B **701**, 186 (2011).
[36] ATLAS Collaboration, Report No. ATLAS-CONF-2011-086.
[37] G. Aad *et al.* (ATLAS Collaboration), Phys. Lett. B **710**, 67 (2012); J. High Energy Phys. 11 (2011) 099.

[38] http://www.sciops.esa.int/SA/PLANCK/docs/Planck2013results16.pdf.
[39] K. Nakamura *et al.* (Particle Data Group Collaboration), J. Phys. G **37**, 075021 (2010).
[40] E. Barberio *et al.*, arXiv:0808.1297.
[41] CDF Collaboration, Phys. Rev. Lett. **107**, 191801 (2011); CMS and LHCb Collaborations, Report No. LHCb-CONF-2011-047, and CMS PAS BPH-11-019.
[42] V. M. Abazov *et al.* (D0 Collaboration), Phys. Lett. B **693**, 539 (2010).
[43] S. Akula, D. Feldman, P. Nath, and G. Peim, Phys. Rev. D **84**, 115011 (2011).
[44] G. Belanger, F. Boudjema, A. Pukhov, and A. Semenov, Comput. Phys. Commun. **180**, 747 (2009); G. Belanger, F. Boudjema, P. Brun, A. Pukhov, S. Rosier-Lees, P. Salati, and A. Semenov, Comput. Phys. Commun. **182**, 842 (2011).
[45] B. C. Allanach, Comput. Phys. Commun. **143**, 305 (2002).
[46] S. P. Martin, Phys. Rev. D **79**, 095019 (2009).
[47] D. Feldman, Z. Liu, and P. Nath, Phys. Rev. D **80**, 015007 (2009); N. Chen, D. Feldman, Z. Liu, P. Nath, and G. Peim, Phys. Rev. D **83**, 035005 (2011).
[48] I. Gogoladze, F. Nasir, and Q. Shafi, arXiv:1212.2593.
[49] P. Nath *et al.*, Nucl. Phys. B, Proc. Suppl. **200–202**, 185 (2010).
[50] B. L. Kaufman, B. D. Nelson, and M. K. Gaillard, arXiv:1303.6575.
[51] D. Feldman, K. Freese, P. Nath, B. D. Nelson, and G. Peim, Phys. Rev. D **84**, 015007 (2011).
[52] S. Dimopoulos, S. Raby, and F. Wilczek, Phys. Lett. **1128**, 133 (1982).
[53] J. Ellis, D. V. Nanopoulos, and S. Rudaz, Nucl. Phys. **B202**, 43 (1982).
[54] R. L. Arnowitt, A. H. Chamseddine, and P. Nath, Phys. Lett. **156B**, 215 (1985); P. Nath, A. H. Chamseddine, and R. L. Arnowitt, Phys. Rev. D **32**, 2348 (1985).
[55] J. Hisano, H. Murayama, and T. Yanagida, Nucl. Phys. **B402**, 46 (1993).
[56] T. Goto and T. Nihei, Phys. Rev. D **59**, 115009 (1999).
[57] P. Nath and P. F. Perez, Phys. Rep. **441**, 191 (2007).
[58] S. Raby *et al.*, arXiv:0810.4551.
[59] J. L. Hewett *et al.*, arXiv:1205.2671.
[60] P. Nath and R. L. Arnowitt, Yad. Fiz. **61**, 1069 (1998) [Phys. At. Nucl. **61**, 975 (1998)].
[61] Y. Aoki, C. Dawson, J. Noaki, and A. Soni, Phys. Rev. D **75**, 014507 (2007).
[62] R. Dermisek, A. Mafi, and S. Raby, Phys. Rev. D **63**, 035001 (2000).
[63] D. Emmanuel-Costa and S. Wiesenfeldt, Nucl. Phys. **B661**, 62 (2003).
[64] T. Nihei and J. Arafune, Prog. Theor. Phys. **93**, 665 (1995).
[65] K. Turzynski, J. High Energy Phys. 10 (2002) 044.
[66] H. Murayama and A. Pierce, Phys. Rev. D **65**, 055009 (2002).
[67] P. Nath, and R. M. Syed, Phys. Rev. D **77**, 015015 (2008).
[68] R. L. Arnowitt and P. Nath, Phys. Rev. D **49**, 1479 (1994).
[69] K. S. Babu, J. C. Pati, and Z. Tavartkiladze, J. High Energy Phys. 06 (2010) 084.
[70] K. S. Babu, I. Gogoladze, P. Nath, and R. M. Syed, Phys. Rev. D **85**, 075002 (2012).
[71] K. S. Babu, I. Gogoladze, P. Nath, and R. M. Syed, Phys. Rev. D **72**, 095011 (2005); **74**, 075004 (2006).
[72] R. Barbieri and G. F. Giudice, Nucl. Phys. **B306**, 63 (1988).
[73] P. Ciafaloni and A. Strumia, Nucl. Phys. **B494**, 41 (1997).
[74] G. Bhattacharyya and A. Romanino, Phys. Rev. D **55**, 7015 (1997).
[75] G. W. Anderson, D. J. Castaño, and A. Riotto, Phys. Rev. D **55**, 2950 (1997).
[76] G. L. Kane and S. F. King, Phys. Lett. B **451**, 113 (1999).
[77] P. H. Chankowski, J. R. Ellis, M. Olechowski, and S. Pokorski, Nucl. Phys. **B544**, 39 (1999).
[78] J. A. Casas, J. R. Espinosa, and I. Hidalgo, J. High Energy Phys. 01 (2004) 008.
[79] S. P. Martin, Phys. Rev. D **83**, 035019 (2011).
[80] N. Arkani-Hamed, K. Blum, R. T. D'Agnolo, and J. Fan, J. High Energy Phys. 01 (2013) 149.
[81] D. M. Ghilencea, H. M. Lee, and M. Park, J. High Energy Phys. 07 (2012) 046.
[82] J. Jaeckel and V. V. Khoze, J. High Energy Phys. 11 (2012) 115.
[83] H. Baer *et al.*, arXiv:1212.2655.
[84] D. McKeen, M. Pospelov, and A. Ritz, arXiv:1303.1172.
[85] C. Boehm, P. S. B. Dev, A. Mazumdar, and E. Pukartas, arXiv:1303.5386.